POLYPUBLIE
Polytechnique Montréal

POLYTECHNIQUE MONTRÉAL
UNIVERSITÉ D'INGÉNIERIE

Titre: Numerical investigation of the stability of a base-exposed sill mat made of cemented backfill
Title:

Auteurs: Philippe Pagé, Li Li, Pengyu Yang, & Richard Simon
Authors:

Date: 2019

Type: Article de revue / Article

Référence: Pagé, P., Li, L., Yang, P., & Simon, R. (2019). Numerical investigation of the stability of a base-exposed sill mat made of cemented backfill. International Journal of Rock Mechanics and Mining Sciences, 114, 195-207. https://doi.org/10.1016/j.ijrmms.2018.10.008
Citation:

Document en libre accès dans PolyPublie
Open Access document in PolyPublie

URL de PolyPublie: https://publications.polymtl.ca/3825/
PolyPublie URL:

Version: Version finale avant publication / Accepted version
Révisé par les pairs / Refereed

Conditions d'utilisation: CC BY-NC-ND
Terms of Use:

Document publié chez l'éditeur officiel
Document issued by the official publisher

Titre de la revue: International Journal of Rock Mechanics and Mining Sciences (vol. 114)
Journal Title:

Maison d'édition: Elsevier
Publisher:

URL officiel: https://doi.org/10.1016/j.ijrmms.2018.10.008
Official URL:

Mention légale: © 2019. This is the author's version of an article that appeared in International Journal of Rock Mechanics and Mining Sciences (vol. 114) . The final published version is available at https://doi.org/10.1016/j.ijrmms.2018.10.008. This manuscript version is made available under the CC-BY-NC-ND 4.0 license https://creativecommons.org/licenses/by-nc-nd/4.0/
Legal notice:

Ce fichier a été téléchargé à partir de PolyPublie, le dépôt institutionnel de Polytechnique Montréal
This file has been downloaded from PolyPublie, the institutional repository of Polytechnique Montréal

https://publications.polymtl.ca

Numerical investigation of the stability of a base-exposed sill mat made of cemented backfill

Philippe Pagé[1], Li Li[1], Pengyu Yang[2,1*], Richard Simon[1]

[1]Research Institute on Mines and Environment

Department of Civil, Geological and Mining Engineering

École Polytechnique de Montréal

C.P. 6079 succursale Centre-ville, Montreal, Quebec, Canada H3C 3A7

[2]School of Architecture and Civil Engineering

Xi'an University of Science and Technology

58 Yanta Rd., Xi'an, 710054 China

[*]Corresponding author. E-mail: pengyu.yang@polymtl.ca

Manuscript accepted to be published in the *International Journal of Rock Mechanics and Mining Science*

Submitted: April 2018

Resubmitted: August 2018

Accepted: October 2018

Numerical investigation of the stability of a base-exposed sill mat made of cemented backfill

Philippe Pagé, Li Li, Pengyu Yang*, Richard Simon

Abstract: Sill mats are important supporting structures commonly applied in underground mines for better recovery. They are used to help recover sill pillars in open stoping or to provide a safer workplace in underhand cut-and-fill mining. To fulfil these functions, the sill mat is typically cast with cemented backfill mainly consisting of mine tailings and binders. To ensure economic and safe mining, a critical issue is to estimate the required strength of the base-exposed sill mat following underneath extraction. So far, a few analytical solutions have been proposed for this purpose by treating the sill mat as an isolated bending beam with two fixed ends. However, previous numerical analyses have indicated that the response of the sill mat can be significantly influenced by the rock wall closures due to underneath extraction. This aspect is ignored by the existing analytical models. In this paper, numerical models are used to evaluate the stability of sill mats upon the underneath excavation. The influence of rock wall closure on the stability and the minimum required strength of sill mats is analyzed. Simulation results indicate that the apparent failure mechanism of the sill mat is caving or rotation, while its actual failure mechanism is crushing or shearing. Accordingly, the required strength of sill mats increases as the variation of studied influencing factors tends to increase the horizontal stresses in the sill mats, including the increase in mine depth, rock pressure coefficients and sill mat stiffness. In contrary, the increase in the span or thickness of sill mat and rock mass stiffness tends to decrease the horizontal stresses in the sill mat, thereby leading to a reduction in the required strength of sill mats. It is also concluded that the stress increase does not always mean an improvement or deterioration of the stability of the sill mats.

Key-words: Sill mat; Cemented backfill; Minimum required strength; Numerical modeling; Stability

*Corresponding author. E-mail: pengyu.yang@polymtl.ca

1. Introduction

Stope backfilling has been widely applied in underground mines worldwide. This practice can not only help reduce the environmental impact of mining operations, but also serves to improve ground stability, provide a safer workspace, reduce ore dilution, and help control the airflow.[1-3] A sill mat made of cemented backfill is commonly used to recover sill pillars in open stoping methods or to provide a safer workplace in underhand cut-and-fill mining method.[3,4-6] A critical issue is to correctly estimate the minimum required strength of cemented backfill used to construct the sill mat to ensure the stability of the sill mat upon base exposure due to subsequent undercutting.

This issue has been treated by Mitchell[7], who considered a sill mat with an overlying cohesionless backfill confined by two stiff and immobile walls. Based on limit equilibrium analyses, Mitchell[7] proposed a series of analytical solutions to evaluate the stability of an unreinforced sill mat based on four types of failure mechanisms: sliding, rotation, flexure and caving. To verify his analytical model, Mitchell[7] conducted a series of experimental tests with a centrifuge. The four failure modes assumed by Mitchell[7] were observed in his centrifuge tests. More details of the centrifuge model tests are recalled in the section of Discussion (see below).

Oulbacha[8] evaluated the correctness of the Mitchell[7] solutions using a limit equilibrium code. His simulations results have shown that the Mitchell solutions cannot always provide good predictions on the stability of sill mats. For sliding failure, good correlations have been obtained between his numerical results and the Mitchell solution. For rotational failure, the numerical simulations performed by Oulbacha[8] have shown that the Mitchell solution generally tends to underestimate the sill mat stability; similar results have been previously reported by Caceres[9]. However, when the stope walls are not inclined enough from the vertical, Oulbacha[8] has shown that the upper contact corner between the sill mat and the hanging wall has to be sheared before the occurrence of rotation failure. The stability of the sill mat is further underestimated by the analytical solution of Mitchell[7]. For flexural failure, Oulbacha[8] has shown that the Mitchell solution is valid for stopes inclined within 20° from the vertical. Through numerical modeling with extremely high sill mat cohesion (c = 60 MPa), Caceres et al.[10] further indicated that the Mitchell solution for flexural failure can be valid only if sill mats have very large span to thickness ratios (i.e., > 6.7). As for caving failure, Oulbacha[8] has demonstrated that the Mitchell solution largely overestimates the stability of the sill mat in the case of large cohesion and slightly underestimates the stability of the sill mat in the case of low cohesion.

Over the years, the Mitchell[7] solutions for the design of sill mats have recognized less applications compared to their very successful Mitchell et al.[11] solution for designing the side-exposed backfill, due probably to several over-simplified assumptions associated with the former. For instance, a normal confining stress contained in the analytical solutions of Mitchell[7] is undetermined. In addition, the sill mat was assumed as an isolated bending beam with two fixed ends. The effect of underlying excavation on the sill mat was not considered. In reality, the rock walls upon underneath excavation may deform and compress the sill mat. Numerical models conducted by Sobhi and Li[12] have shown that the stress state within the sill mat and overlying backfill can be significantly altered by the wall closure induced by the underlying excavation. Centrifuge tests performed by Dirige and De Souza[13] also indicated that excavation width, wall roughness and wall closure influence the stability of sill pillars. It is thus important to take into account the effect of wall closure on the stability of sill mats. However, the closure of stope walls depends on several factors, such as the mechanical properties of sill mats and rock mass, geometry of stope and sill mats, in-situ stresses, etc. It would be too time-consuming and expensive to evaluate the influence of these factors through physical model tests.

Numerical modeling has been proven to be a useful and cost-effective tool to treat diverse complicated problems in geotechnical/mining engineering. For example, Brummer et al.[14] used FLAC 3D to estimate the required strength of sill mats as a function of the stope span for different stope inclinations, without the consideration of mine depth and wall closure. Caceres[9] investigated the stability of cemented rockfill sill mat with FLAC 2D. Design curves were developed by considering zero wall convergence and uniform vertical stresses along the top span of the stope. Hughes[15] has numerically derived nine distinct design curves to represent the minimum required *UCS* (unconfined compressive strength) for a given span width by considering a factor of safety (*FS*) of 1.0. For simplicity, the convergences of rock walls were assumed to be 0, 5 and 15 cm, respectively corresponding to mine depths of 400, 800 and 3000 m. The actual wall convergences associated with the in-situ stresses and several influencing factors (e.g. stiffness of the rock mass, stope inclination, the thickness of the sill mat and the height of the overlying backfill) have been neglected. Additionally, the criterion used to judge the failure of the sill mat observed in numerical models was not clearly defined and presented.

To better understand the stability and the required strength of base-exposed sill mat (overlain by an uncemented backfill) submitted to diverse conditions, a series of numerical simulations have been done with Plaxis 2D.[16] In this paper, a part of the numerical results is presented. The influences of the mine depth, stope and sill mat geometries, and mechanical properties of the sill mat and rock mass on the required cohesion of the cemented sill mat are analysed and discussed.

2. Numerical models

In this study, the finite element code Plaxis 2D[16] is used to assess the stability of the sill mat upon excavation underneath. Its validation has been shown by Sobhi[17] and Pagé[18]. Plaxis 2D has been used by the authors and others[12,19] to investigate the mechanical behavior of mine backfill in various conditions.

2.1 Model configuration

The schematic model of a sill mat with an overlying uncemented backfill and an underneath excavation is illustrated in Fig. 1a. On the figure, W (m) is the width of the stope or span of the sill mat, H (m) is the height of the overlying backfill, e (m) is the thickness of the sill mat, and β (°) is the inclination angle (to the horizontal) of the stope walls. A void space (0.5 m high) is left on top of the uncemented backfill to simulate the case of poor contact between the backfill and stope roof. In some cases, depending on the mining method, a void space with a height of drift (3 to 5 m high) can be necessary to allow the passage of vehicles and workers.

Fig. 1 also shows numerical models of a vertical (Fig. 1b) and an inclined (Fig. 1c) stope – sill mat system built with Plaxis 2D before the excavation of the underlying stope. Only half of the model is simulated by considering the plane of symmetry ($x = 0$) for vertical stopes ($\beta = 90°$) while full model is simulated in the case of inclined stopes ($\beta < 90°$). For both cases, the top boundary is set free to simulate the ground surface, while only vertical displacement is allowed along the two side outer boundaries. The lower outer boundary is fixed in all directions. The backfill and sill mat are modeled as elasto-plastic Mohr-Coulomb materials while the rock mass obeys the generalized Hoek-Brown criterion. Point X is marked as the bottom center of the sill mat.

The vertical stope along with the geometry and material property parameters shown in Fig. 1b is taken as the reference (base) case, in which the overlying backfill has a height $H = 9.5$ m, a Young's modulus $E = 250$ MPa, a Poisson's ratio $\mu = 0.3$, a unit weight $\gamma = 18$ kN/m^3, a friction angle $\phi = 25°$, and a dilation angle $\psi = 0°$. The sill mat has a width $W = 6$ m, a thickness $e = 3$ m, a Young's modulus $E_s = 1$ GPa, a Poisson's ratio $\mu_s = 0.3$, a unit weight $\gamma_s = 19$ kN/m^3, a cohesion

c_s = 2000 kPa, a friction angle ϕ_s = 30°, and a dilation angle of ψ_s = 0°. Published works on laboratory tests have shown that the tensile strength of cemented fill is typically around 1/10 of the UCS.[20,21] The following expression is then used to estimate the tensile strength σ_t of sill mat from the cohesion c_s, based on the Mohr-Coulomb criterion:

$$\sigma_t = \frac{c_s}{5} \tan(45° + \phi_s/2) \quad (1)$$

With c_s = 2000 kPa and ϕ_s = 30°, Eq. (1) gives a tensile strength of σ_t = 692 kPa in the reference case.

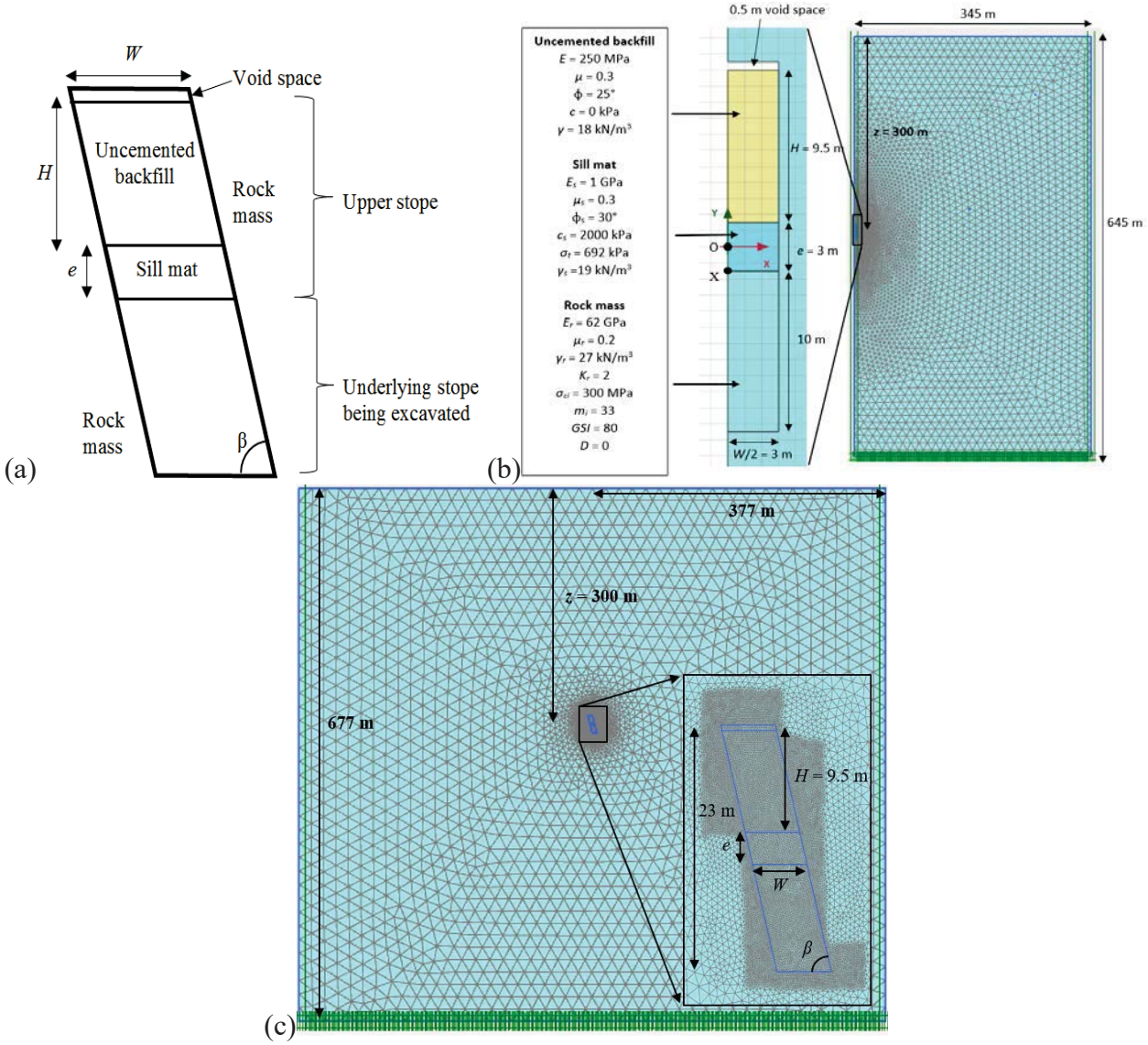

Fig. 1. (a) Schematic view of an undercut below a sill mat overlain by an overlying uncemented backfill; Numerical models of (b) a vertical and (c) an inclined stope - sill mat system built with Plaxis 2D.

For the reference case, the surrounding rock mass has a Young's modulus E_r of 62 GPa, a Poisson's ratio μ_r of 0.2, a unit weight γ_r of 27 kN/m^3, a geological strength index *GSI* of 80, and a damage index D of 0 (without disturbance). The Hoek-Brown parameters for the intact rock (extremely strong) are σ_{ci} = 300 MPa (uniaxial compressive strength) and m_i = 33 (s = 1 implicitly). Such high strength values are used to ensure that the rock mass does not yield and the stability analyses are focused on that of the sill-mat. The mine depth is measured as z = 300 m between the

ground surface and mid-height of the sill mat. A typical stress regime of the Canadian Shield is applied to the rock mass with the lateral earth pressure coefficient $K_r = 2$.[22] The horizontal natural stress is then twice the vertical in-situ stress that is equal to the vertical stress based on the overburden solution.

The sequence of excavation and backfilling performed in Plaxis 2D are identical for vertical (Fig. 1b) and inclined stopes (Fig. 1c). The first step is to establish an initial stress state within the rock mass, followed by the excavation of the upper stope. The induced displacements in the rock mass are reset to zero to simulate the release of the elastic and plastic deformations on the surrounding rock. A sill mat made of cemented backfill is then constructed, followed by adding a single layer of cohesionless backfill above the sill mat. The last step is to remove the underlying stope below the sill mat. Figure presentation of the excavation and filling sequence can be found in Sobhi and Li[12] and Pagé[18]. Table 1 summarizes the characteristics of all simulation cases performed in this investigation.

Table 1. Characteristics of the different simulations cases (with $E = 250$ MPa, $\mu = 0.3$, $\phi = 25°$, $c = 0$ kPa and $\gamma = 18$ kN/m^3 for the uncemented backfill, $\gamma_s = 19$ kN/m^3, $\mu_s = 0.3$ and $\phi_s = 30°$ for the cemented sill mat, $\gamma_r = 27$ kN/m^3, $\mu_r = 0.2$, $m_i = 33$, $GSI = 80$ and $D = 0$ for the rock mass).

Case	Figures	Stope geometry		Sill mat		Rock mass			Backfill
		β (°)	W (m)	e (m)	E_s (GPa)	E_r (GPa)	K_r	σ_{ci} (MPa)	H (m)
0	3 and 4	90	6	3	1	62	2	300	9.5
1	5 to 7	VAR	6	3	1	62	2	300	9.5
2	8 to 10	90	VAR	3	1	62	2	300	9.5
3	11a	90	6	VAR	1	62	2	300	9.5
4	11b	90	6	3	VAR	62	2	300	9.5
5	12a	90	6	3	1	VAR	2	300	9.5
6	12b	90	6	3	1	62	VAR	300	9.5
7	13	90	6	3	1	62	2	300	VAR

2.2 Instability indicator of the sill-mat

To determine the minimum (i.e., $FS = 1$) required strength of a sill mat, a series of numerical simulations are done by reducing its cohesion c_s to a sufficiently low value so that the failure/instability of the sill mat can be observed. Until now, most numerical analyses evaluated the instability of a structure through the examination of yield state.[9,10,14,15,23,24] When a massive material yielding occurs at critical places, one can pronounce with high degree of confidence that the structure becomes instable. In many cases, one may observe minor material yielding at punctual and local places. It may be concluded that the structure becomes instable and would fail due to possible development or propagation of yielding around the yield portions. Conversely, it may also be concluded that the structure remains stable as the yielding is only minor and local. The residual strength plays a role of stabilisation and the punctual and local yielded material does not affect the global stability of the structure. This concept has generally been accepted in slope stability analyses.[25,26] These indicates that the evaluation of the stability of a structure based on yielding can sometimes be subjective.

Dirige and De Souza[13] have shown that the displacement can sometimes provide useful information on the state of the backfill even though they did not evaluate the critical (minimum required) strength of sill-mat. Recently, Yang et al.[27,28] and Liu et al.[29] have shown that the subjectivity in assessing the stability or instability of structures (barricade and side-exposed backfill) can be reduced by monitoring the displacements at some critical points. In this study, the

total displacement at the bottom (center Point *X* for vertical stopes; see Fig. 1b) of the sill mat is monitored. Displacement at other points have also been monitored (see details presented in Pagé[17]). It has been shown that the displacement of Point *X* represents the maximum value along the base of a sill mat, and thus deemed representative of the global stability.

Fig. 2a shows the variation of the displacement at Point *X* (negative values indicate the downward displacements) as a function of the sill mat cohesion c_s. When the value of c_s reduces from 2 MPa to 500 kPa, the numerical calculations converge to small and almost constant displacements, indicating a stable sill mat. The displacement starts to significantly increase as c_s is reduced to 400 kPa and increases dramatically once the value of c_s is below 400 kPa, indicating an unstable sill mat. The critical (minimum) required cohesion should be a value between 400 (unstable) and 500 kPa (stable) based on the full curve of the displacement as the sill mat cohesion varies from 2 MPa to 71 kPa. However, if one examines the displacement curve as the sill mat cohesion changes from 2 MPa to 300 kPa, one can conclude that the critical cohesion should be a value between 500 kPa (unstable) and 1 MPa (stable). The monitoring of the displacement alone does not allow a clear and objective determination of the critical cohesion c_s.

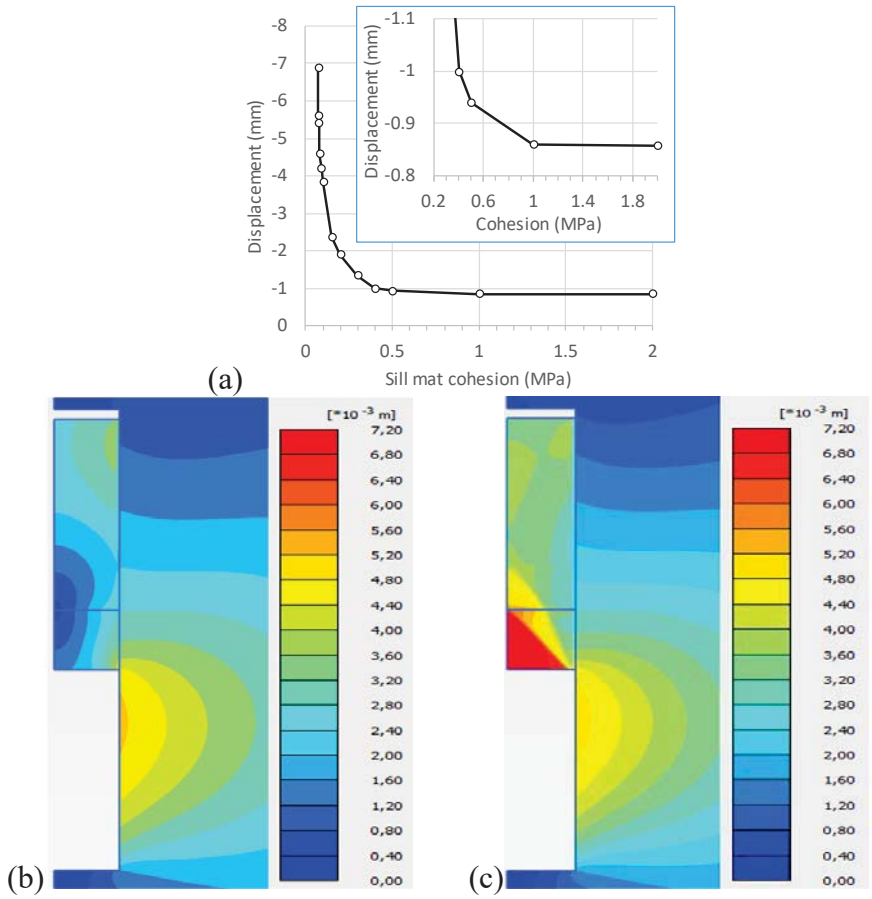

Fig. 2. (a) Variation of the vertical displacements at the bottom center (Point *X*, Fig. 1a) of the sill mat as a function of its cohesion c_s upon base exposure; Iso-contours of total displacements of the stope-sill mat system after removing the underlying stope for (b) c_s = 2000 kPa and (c) c_s = 72 kPa. (Table 1, Case 0 with z = 300 m).

Fig. 2 also shows the displacement contours of the stope – sill mat system for the reference case when the cohesion c_s changes from 2000 kPa (Fig. 2b) to 72 kPa (Fig. 2c). One sees that the sill

mat changes from a stable state at c_s = 2000 kPa to an instable state at c_s = 72 kPa with the formation of a triangular wedge (indicating larger displacement). The latter tends to indicate the caving failure mechanism of the sill-mat. However, if one observes the yield state of the sill mat, it will be shown below that the actual failure mechanism is horizontal crushing or shearing due to the horizontal compression associated with the rock wall closure upon base exposure of the sill mat.

Fig. 3 shows the yield states of the sill mat for the reference case when the cohesion c_s changes from 2000 kPa (Fig. 3a), 500 kPa (Fig. 3b), 400 kPa (Fig 3c) to 72 kPa (Fig. 3d). One notices that points of plasticity due to shear yield start to propagate through the sill mat when the cohesion c_s is reduced to 500 kPa. This propagation increases as the cohesion c_s is further decreased from 400 kPa to 72 kPa with the appearance of tension failure. For sill mat design, the cohesion of 500 kPa can be considered as the minimum required cohesion for the sill mat considered in this case. The displayed failure is caving with a falling wedge, but the governing failure mechanism is shear yield due to crushing of the backfill by the horizontal closure of the rock walls. This failure mechanism was not considered in the Mitchell[7] model.

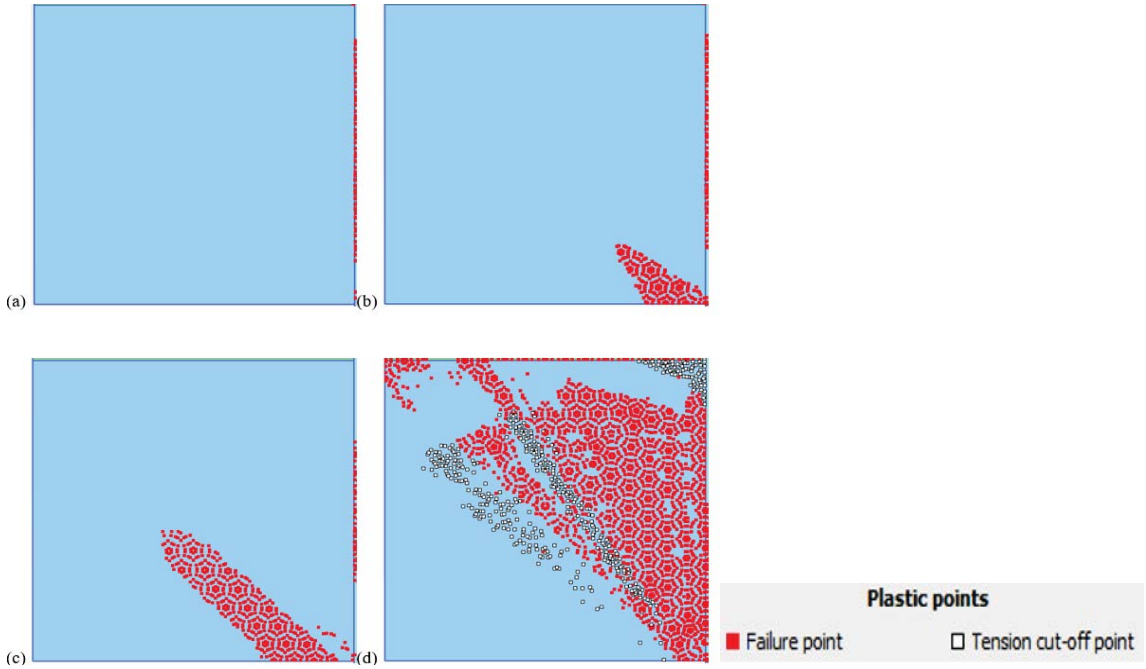

Fig. 3. Propagation of the plasticity points through the sill mat for a variation of the critical cohesion c_s from (a) 2000 kPa; (b) 500 kPa; (c) 400 kPa and (d) 72 kPa for the sill mat located at a depth of z = 300 m for the reference case (Case 0 in Table 1).

Attempt has also been done by considering the distribution of displacements and stresses along the vertical centerline and walls of the sill mat. Sobhi and Li[12] have shown dramatic falls of stresses from the elastic (intact) zone to the yielded (failed) zone by considering zero tension cut-off for the cemented backfill in their numerical models. This is however not the case here probably due to the non-zero tension cut-off for the cemented sill mats.

In the following sections, the minimum required cohesion of the cemented sill mat is determined by considering the total displacement monitored at the base center of the sill mats combined with their yield states. The iso-contours of total displacements across the sill mats, which are always taken as the absolute values of total displacements, are only used to show the shape of failed zones of the sill mats.

3. Numerical results

3.1 Effect of the stope geometry

In this sub-section, the influence of the wall inclination angle β and stope width W on the critical (minimum required) cohesion of sill mat will be investigated.

Fig. 4 presents the variation of the critical cohesion c_s of the sill mat as a function of the stope depths z for different stope inclination angles β. One sees that the value of c_s increases as the angle β decreases. The minimum required cohesion for inclined stopes can thus be underestimated by the solutions established for vertical stopes. Also, for a given inclination angle, the minimum required cohesion c_s increases exponentially with the mine depth. This indicates that neglecting the mine depths can lead to over- or under- estimation of the required strength for sill mats.

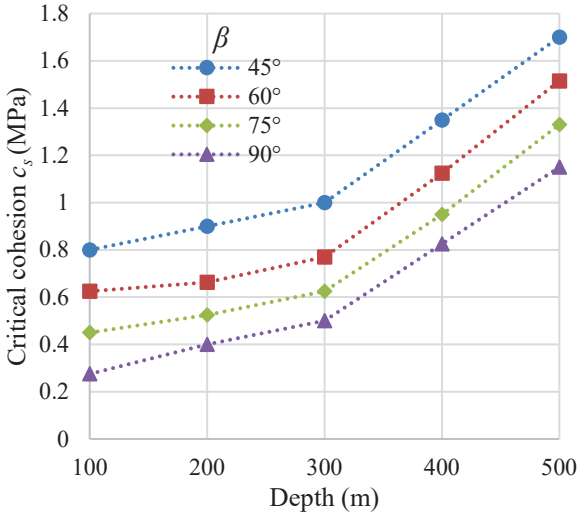

Fig. 4. Variation of the critical cohesion c_s of the sill mat as a function of the mine depths z for different stope inclination angles β (Case 1 in Table 1).

Fig. 5 shows the total displacement vectors and iso-contours of the stope-sill mat system at failure when the stope is located at z = 300 m and the stope inclination angle β varies from 90° (Fig. 5a), 75° (Fig. 5b), 60° (Fig. 5c) to 45° (Fig. 5d). Apparently, the failure mechanism is generally governed by caving for sub-vertical stopes (i.e., $\beta \geq 75°$) or combined rotation and caving for more inclined stopes (i.e., $\beta < 75°$).

Fig. 6 illustrates the states of the sill mats located at z = 300 m at critical cohesion c_s when the stope inclination angle β changes from 90° (Fig. 6a), 75° (Fig. 6b), 60° (Fig. 6c) to 45° (Fig. 6d). One sees that the actual governing failure mechanism is shear yield due to crushing of the backfill by the horizontal closure of the rock walls. The same observations have been obtained for sill mats at any depth between 100 m and 500 m (see more details given in Pagé[17]).

Fig. 7 shows the variation of the critical (minimum required) cohesion of the sill mat as a function of the stope depths for different values of sill mat (and stope) widths W. For a given stope width, one sees that the minimum required cohesion c_s increases slightly with the depth W at shallow depth and significantly increases as the depth further increases. For a given stope depth, the critical cohesion c_s decreases as the stope width W increases. This result is counterintuitive, in particular if the governing failure mechanism is flexure, sliding or rotation. It becomes straightforward once crushing or shearing by compression is recognized as the governing failure mechanism of the sill mat. With wider stope, the compression strain due to the horizontal closure

of rock walls associated with the underneath excavation will be smaller, resulting in lower horizontal stresses and more stable sill mat.

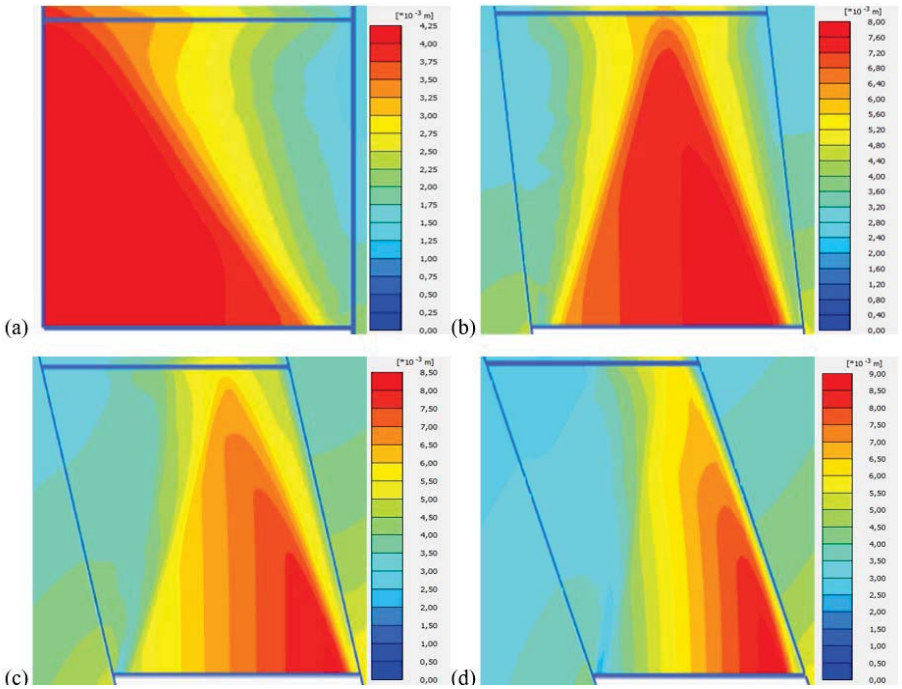

Fig. 5. Vectors and iso-contours of total displacement of the stope-sill mat system (at failure) located at z = 300 m for different stope inclination angles: (a) β = 90°; (b) β = 75°; (c) β = 60°; (d) β = 45° (Case 1 in Table 1).

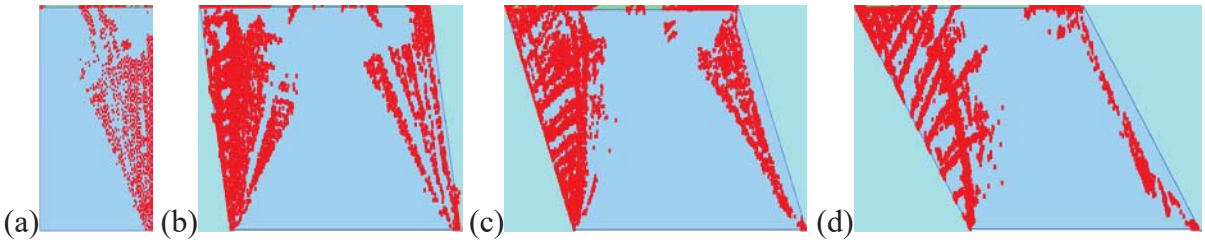

Fig. 6. States of the sill mats located at z = 300 m at critical cohesion c_s for different stope inclination angles: (a) β = 90°; (b) β = 75°; (c) β = 60°; (d) β = 45° (Case 1 in Table 1).

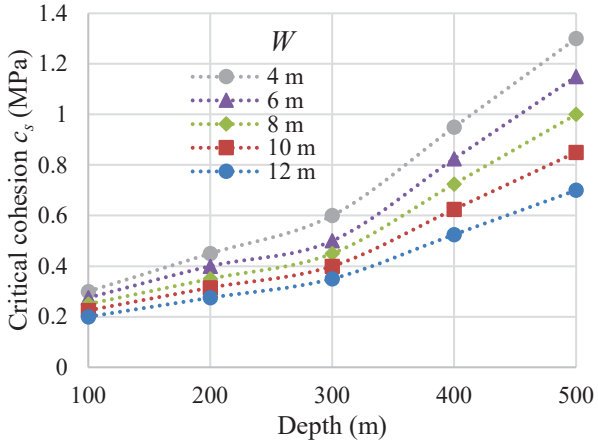

Fig. 7. Variation of the critical cohesion c_s of the sill mat as a function of the mine depth for different stope widths W (Case 2 in Table 1).

Fig. 8 demonstrates the iso-contours of the total displacement of the sill mats at critical cohesion located at z = 300 m when the stope width W varies from 4 to 12 m. Once again, caving is the apparent failure mechanism of the sill mats while shearing or crushing due to the horizontal closure of walls remains the actual governing failure mechanism, as shown in Fig. 9. Subsequently, as the stope width increases, the horizontal strain associated with the wall closure diminishes. The horizontal stresses within the sill mat decreases. The sill mat becomes less prone to crushing failure. The required cohesion diminishes. This also explains well the increase of the required cohesion as the mine depth z increases.

These results could be very different from those predicted by the Mitchell[7] model when the two walls are considered as immobile and the controlled failure mechanism is sliding, flexure or rotation.

Similar results have been obtained for other cases presented in the following sections. Due to space limitation, the iso-contours of displacements and states of sill mats at critical cohesion will not presented; more details can be found in Pagé.[17]

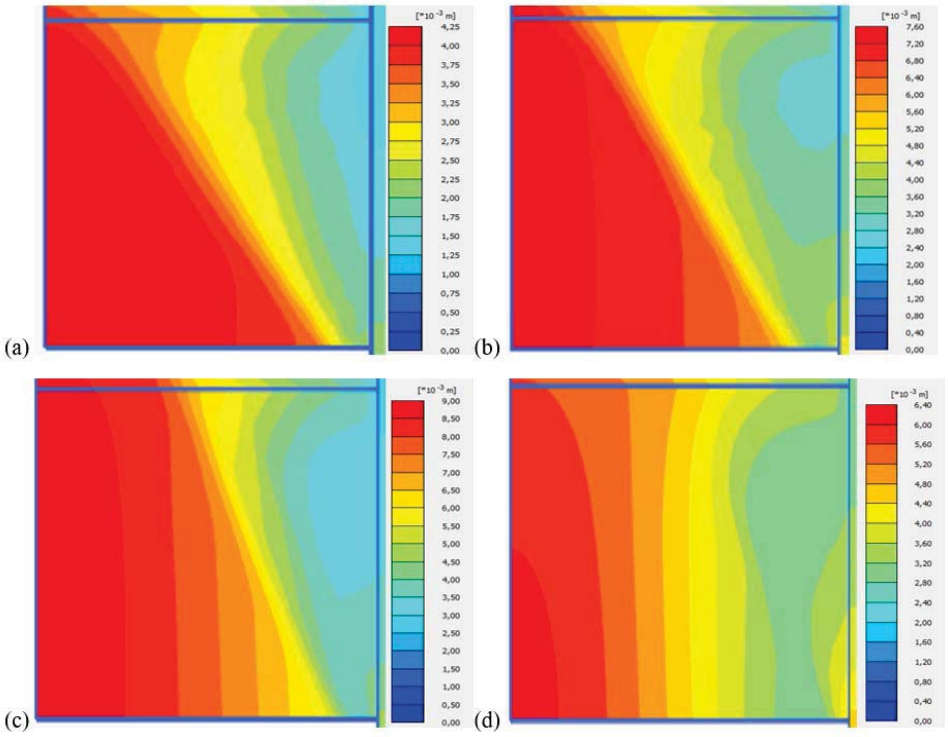

Fig. 8. Iso-contours of total displacement of the sill mats at critical cohesion located at z = 300 m for stope width (not in scale): (a) W = 4 m; (b) W = 8 m; (c) W = 10 m; (d) W = 12 m; other parameters given in Table 1, Case 2.

Fig. 9. State of yield state of the sill mat with the critical cohesion at a mine depth of z = 300 m: (a) W = 4 m, c; (b) W = 8 m; (c) W = 10 m; (d) W = 12 m; other parameters given in Table 1, Case 2.

3.2 Effect of the sill mat thickness and modulus

As stated in previous section, the apparent failure mode can change from one to another, but the actual governed failure mechanism of the sill mat is always crushing or shearing due to the closure of the rock walls. Therefore, it is not necessary to present the iso-contours of displacements and the states of sill mats at the critical cohesion. In the following, only the variation of the required cohesion with different influencing factors will be presented.

Fig. 10 shows the variation of the critical (minimum required) cohesion c_s of the sill mat as a function of stope depths z by considering different thicknesses e (Fig. 10a; Case 3 in Table 1) and Young's modulus E_s (Fig. 10b; Case 4 in Table 1) of sill mats. For a given stope depth, the minimum required cohesion decreases as the thickness e increases from 2 to 8 m. This trend corresponds well to that shown in the abacus of Pakalnis et al.[30] With an increased thickness e, the horizontal stress magnitude decreases in the sill. The crushing or shearing failure due to the closure of the rock wall becomes less possible, resulting in a decreased demand the cohesion. For a given thickness e, the critical cohesion c_s increases with depth as the horizontal stresses in the sill mats increase with the mine depth z.

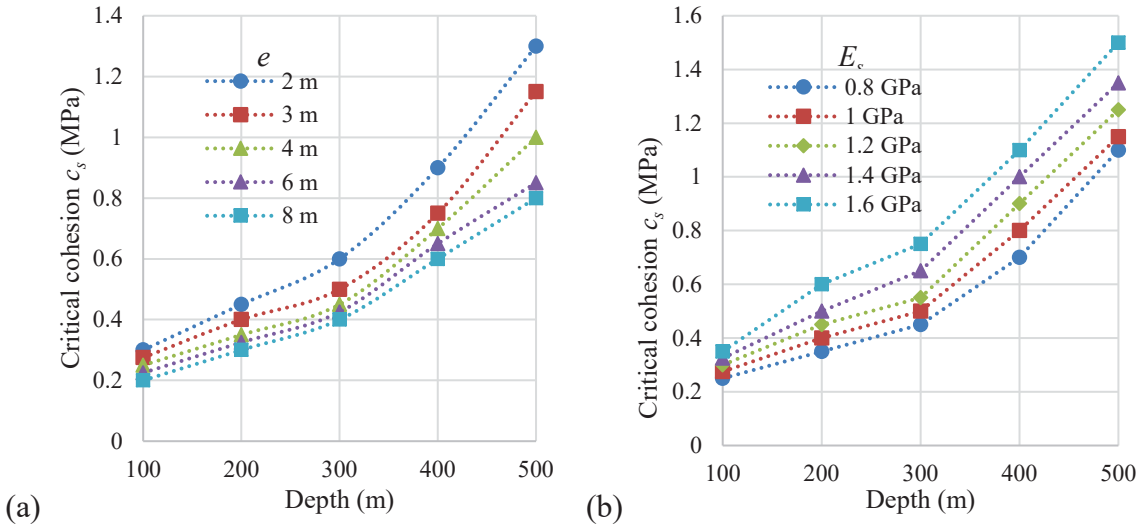

Fig. 10. Variation of the minimum required cohesion of the sill mat as a function of the mine depth by considering: (a) different sill mat thicknesses e (more details given in Table 1, Case 3); (b) different Young's modulus E_s (Case 4 in Table 1).

On the other hand, when the Young's modulus E_s of the sill mat increases, the sill mats are ready to take more charges, resulting in higher stresses in the sill mats. Higher cohesion is needed to avoid the crushing or shearing of the sill mats by the closure of the rock walls. This results in a requirement of higher critical (minimum required) cohesion c_s. For a given modulus, it is straightforward to observe that the required cohesion increases with the stope depth z.

3.3 Effect of the rock mass properties and rock stresses

Fig. 11 illustrates the variation of the critical cohesion of the cemented backfill sill mat at different depths by considering different rock mass properties (Fig. 11a) and rock stresses (Fig. 11b). When the Young's modulus E_r varies from 62 GPa to 82 GPa (Table 1, Case 5), Fig. 11a shows that the critical cohesion c_s decreases. This is quite straightforward. When the rock mass is stiffer and less deformable, the wall closure can be smaller and the resulting stresses in the sill mats

are smaller. The crushing or shearing failure is less possible, resulting in decreased minimum required cohesion. On the other hand, when the mine depth increases, the horizontal stresses in the sill mats increases. Higher cohesion is necessary to counter the crushing or shearing failure, resulting in higher critical cohesion for the cemented backfill.

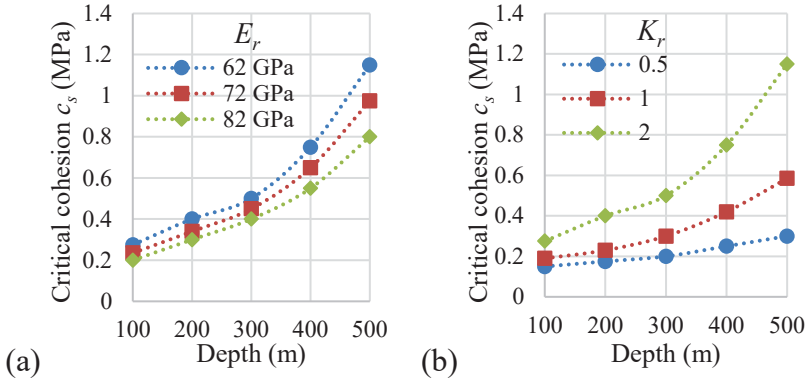

Fig. 11. Variation of the critical cohesion of the cemented backfilled sill mat at different depths by considering different rock mass properties: (a) for different Young's modulus E_r (Case 5 in Table 1); (b) for different rock pressure coefficients K_r (Case 6 in Table 1).

When the rock pressure coefficient K_r increases from 0.5 to 2, the initial horizontal stresses present in the rock mass would largely increase. Accordingly, the final horizontal stresses in the sill mats following the undercut would also undergo a large rise. As illustrated in Fig. 11b (Table 1, Case 6), when the value of K_r increases from 0.5 to 2, the value of the required cohesion c_s has to be increased due to the increased crushing or shearing exerted on the sill mats by the rock walls.

3.4 Effect of height of the overlying backfill

Fig. 12 shows the variation of the critical (minimum required) cohesion c_s of the sill mat as a function of stope depths z for different values of the backfill height H (Case 7 in Table 1). For a given stope depth, the minimum required cohesion c_s increases significantly as the backfill height H increases from 9.5 to 28.5 m. This is also straightforward. With a higher overlying stope, more confining stresses along the overlying stope are released. More rock stresses are then transferred on the sill mats, resulting in higher horizontal stresses in the sill mats. Higher strength is necessary to avoid crushing or shearing failure of the sill mats.

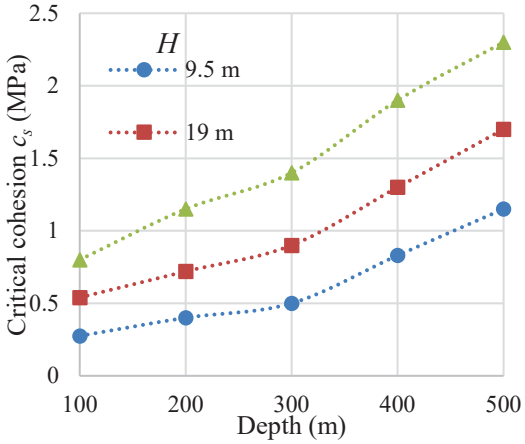

Fig. 12. Variation of the minimum required cohesion of the sill mat as a function of the mine depths for different height of the backfill H (more details given in Table 1, Case 7).

4. Discussion

Numerical simulations have been conducted to evaluate the stability of a sill mat exposed at base with an overlying uncemented backfill upon undercut. A non-zero tension cut-off is used to represent the tensile strength of the cemented fill. The critical cohesion c_s of the exposed sill mat was assessed by considering the displacements and yield state of the sill mats. An unusual failure mode is revealed by the numerical models, which is the crushing or shearing yield of the sill mats by excessive horizontal stresses associated with the closure of rock walls. With this mechanism of failure, the increase of a stress in the sill mat does not always mean an improvement or deterioration of the stability. An increase of the horizontal stress tends to decrease the stability if the controlled failure mechanism is horizontal crushing but increase the stability if the flexural failure governs. Similarly, the increased vertical stresses (exercised by the overlying uncemented backfill) tend to destabilize the sill mats if the flexure controls the stability, while the increased vertical stresses tend to stabilize the sill mats in the case of horizontal crushing as they play a role of confining pressure. Accordingly, the variations in stresses and displacements (see details presented in Pagé[17]) do not provide more useful information to help identify the transition from an intact state to failure state of the sill mats.

The failure of sill mat by crushing or shearing yield has also been reported by Hughes[15] for the simulated cases when the mine depth is greater than 800 m. For stopes at depth less than 400 m, however, rock wall convergence was considered as zero by Hughes.[15] This study showed that rock wall convergence takes place at any mine depth and crushing or shearing is the actual failure mechanism. The increased critical cohesion with increased mine depth and decreased stope width can readily be understood through this new failure mechanism.

4.1 Comparisons with the abacus of Pakalnis et al.[30]

Pakalnis et al.[30] have made use of an abacus proposed by Stone[31] to determine the required *UCS* as a function the stope span for different thicknesses of sill mats by considering a factor of safety of 2. The influence of mine depth is not considered by the abacus of Pakalnis et al.[30]

Fig. 13a presents a comparison between the required *UCS* obtained with the abacus of Pakalnis et al.[30] and those obtained by numerical modeling with Plaxis 2D for the case of sill mats having a thickness e of 3 m. The critical cohesions c_s of the numerical results were converted to *UCS* through $UCS = 2c_s \tan(45° + \phi_s/2)$. The Pakalnis et al.[30] abacus requires higher strength with wider sill mat while the numerical model shows a general decrease of the required strength with larger stope span. Again, this difference is attributed to the fact that the abacus of Pakalnis et al.[30] was established by considering flexure failure of sill mats without considering the wall closure while the numerical modeling presented in this study accounted for the closure of rock walls and the governing failure mechanism of the sill mats is crushing and shearing. The required *UCS* based on the abacus of Pakalnis et al.[30] are underestimated for narrow stope and overestimated for wide stope.

Fig. 13b presents another comparison between the required *UCS* obtained with the abacus of Pakalnis et al.[30] and those obtained by numerical modeling with Plaxis 2D for the case of sill mats having a span W of 6 m. One can see that the Pakalnis et al.[30] abacus and the numerical models predict smaller required *UCS* as the thickness e increases. Again, the abacus of Pakalnis et al.[30] does not consider the influence of mine depth. It generally underestimates the required strength for thick sill mats. With sill mats having relatively small thickness, the abacus of Pakalnis et al.[30] tends to underestimate the required strength when the mine depth is large and overestimate the required strength when the mine depth is small.

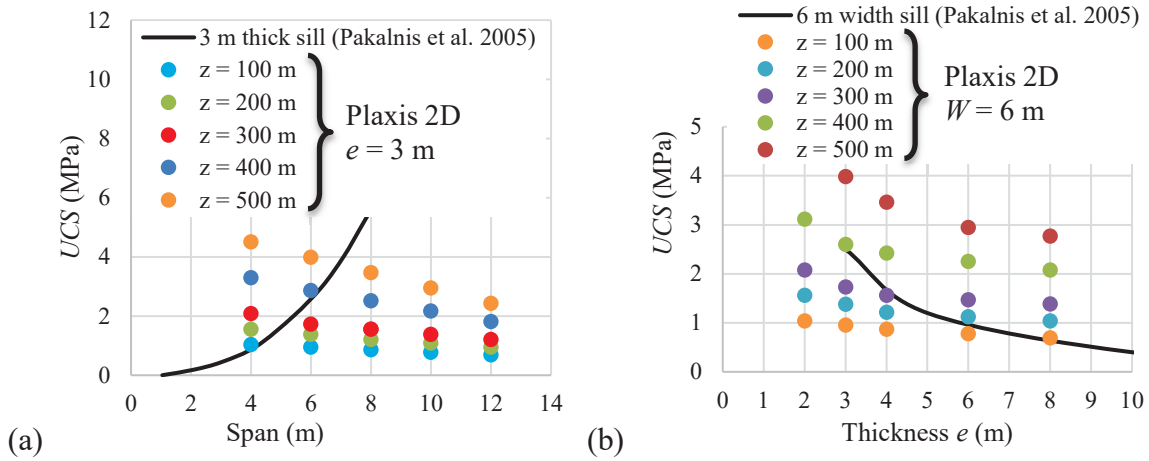

Fig. 13. Comparisons between numerical results obtained with Plaxis 2D and curves of Pakalnis et al.[30] in terms of required *UCS* implying a FS = 2: (a) for a 3 m thick sill having different widths *W*; (b) for sill mats having a span of 6 m. Calculations made with $\phi_s = 30°$ and with the critical cohesion values found in Figs. 7 and 10a.

4.2 Comparisons between numerical models and laboratory tests

The validation of Plaxis 2D has been first checked against analytical solutions proposed for the problem of a cylinder hole.[32,33] The applicability of the numerical model is further tested by reproducing some centrifuge tests performed by Mitchell.[7]

Two centrifuge model tests (named as C2 and C3 by Mitchell[7]) performed on unreinforced cemented sill mats were reproduced. The stope walls are inclined at an angle of 70° to the horizontal. The sill mats have a thickness *e* and a width *W*, overlain by an uncemented fill with a thickness of at least 250 mm. The third dimension of the sill mat (perpendicular to the paper plane) is estimated as 1.2 times the thickness *e*. Table 2 shows the characteristics of the two simulated centrifuge model tests. The small ratios of the third dimension of the sill mat to its width (about 0.5) indicate that the 2D numerical models are not very appropriate for simulating these two centrifuge model tests, if the frictions between the backfills and the front and back walls are not negligible.

In the physical model of Mitchell[7], a scale factor λ is defined as the ratio of the centrifugal acceleration *a* over the gravitational acceleration *g*, with λ_{max} indicating the scale factor at failure.

In the numerical models with Plaxis 2D, the scale factor λ is considered by attributing a density of $\lambda\rho$ to the backfill; where ρ is the actual density of the backfill. The cohesion *c*, the *UCS*, and the tensile strength σ_t were given in Mitchell[7] for each model. Several try, and error tests have been done to find the necessary but unknown parameters. The Young's modulus for the sill mat in model C2 and C3 are respectively estimated to be 900 MPa and 140 MPa. The uncemented backfill overlying the sill is estimated to have a Young's modulus of 70 MPa for all models. The angle of friction for the uncemented backfill was set at 33° while the angle of friction for both sill C2 and C3 was set 35° for both sill model C2 and C3. The interface properties along the hanging wall and foot wall were estimated to be $c_i = 90$ kPa and $\phi_i = 25°$ for model C2 and $c_i = 420$ kPa and $\phi_i = 14°$ for model C3.

Fig. 14a illustrates the variation of total displacements at the middle bottom of the sill mat as a function of the scale factor λ for the model test C3. It can be observed that the total displacement increases with the numerical scale factor λ up to 120. Beyond this value, there is a sudden increase in the total displacements until $\lambda = \lambda_{max} = 124$, indicating the failure of the sill mat. This value is

very close to the experimental results of $\lambda = \lambda_{max} = 125$. Similar results were obtained for model tests C2 with the scale factor at failure of 36 for model test and 35 in the numerical modeling.

Table 2: Characteristics of the centrifuge model tests, performed by Mitchell[7], reproduced numerically with Plaxis 2D.

Test	β (°)	e (mm)	e/W	Scale factor at failure λ_{max}		Failure modes in tests	Failure modes in Plaxis 2D
				Test	Plaxis 2D		
C2 (20/1[1])	70	35	0.43	35	36	Caving, cracking	Caving, cracking
C3 (7/1[1])	70	25	0.4	125	124	Sill rotation	Sill rotation

Note: [1]: ratio of dry tailings to cement; λ_{max}: scale factor at failure.

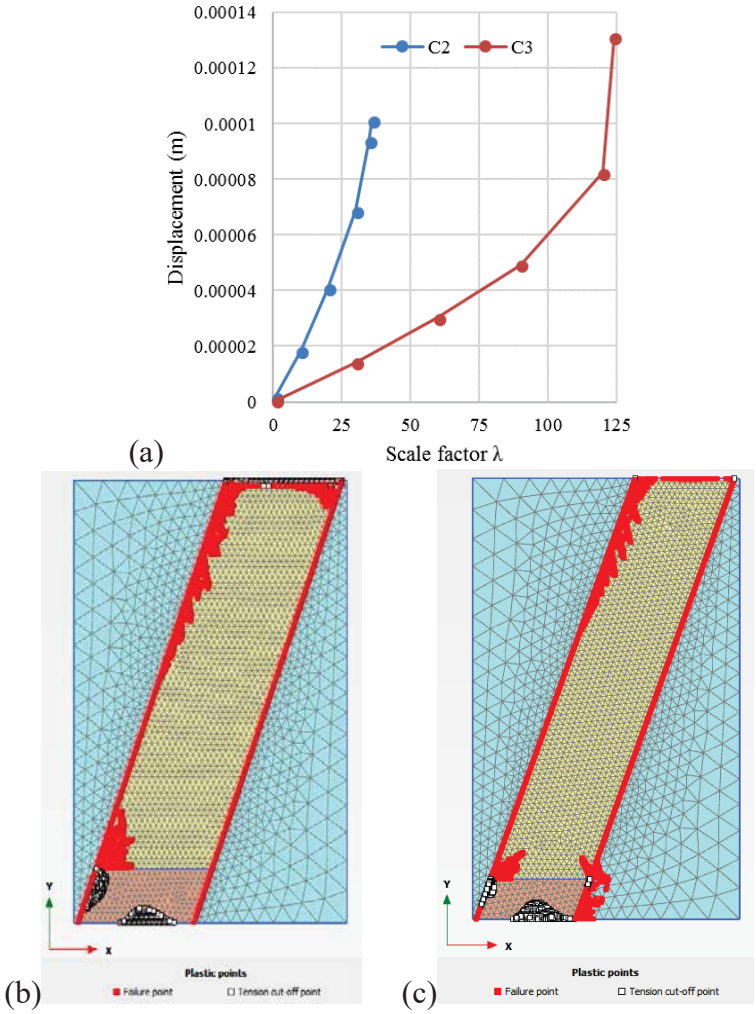

Fig. 14. (a) Variation of displacements with the scale factor λ for the model tests C2 and C3; Yield states of the sill mat and the overlying uncemented backfill obtained from numerical simulations for model (b) C2 and (c) C3 (see Table 2 for details).

Figs. 14b and 14c show the yield state of the sill mats and uncemented backfill, obtained by the numerical simulations for model tests C2 and C3. For both cases, caving by tension is observed near the bottom of the sill mat. Tension along the sill-hanging wall interface indicates that the

detachment of the backfill is possible. The initial failure mode should be caving and rotation. When the caving portion falls, the failure can propagate upward and throughout the sill mat, as observed during the model tests performed by Mitchell[7]. The numerical models can thus be considered as partly verified by the laboratory test results of Mitchell[7].

4.3 Limitations

The numerical modeling has been done without considering interface elements between the sill mat (and overlying backfill) and stope walls. For most cases, the rock walls are irregular and rough due to production blasting. The consideration of interface elements is not necessary.[34] In the case of planar walls, the non-consideration of interface elements implies the anchorage of sill mats to the stope walls. Otherwise, interface elements must be considered in the numerical models.[35]

The numerical models presented in this paper are based on a 2D numerical code by considering plane strain condition. The results are valid for the case of very long stopes in the third dimension. In the future, 3D numerical modeling is necessary to evaluate the impact of the third dimension.

In this study, the elastoplastic Mohr-Coulomb model was used to represent the backfill. The Mohr-Coulomb criterion has been extensively used in geotechnical engineering, mostly due to its simplicity.[23,28,36,37] However, it is not always fully representative of cohesive geomaterials, such as cemented backfill, when dealing with tensile or high compression stresses.[15] More elaborated constitutive models should be used to better investigate the behavior of cemented backfill.[38,39]

5. Conclusions

The stability of a sill mat was analyzed by the pioneer Mitchell, who considered stiff and immobile walls in both the analytical model and physical tests. No wall closure was considered. Four failure mechanisms of the sill mat were identified: sliding, flexure, rotation, and caving. In this study, the sill mat upon base-exposure is numerically analyzed with Plaxis 2D. Mine depth and the effect of the excavation below the sill mats were considered. The critical cohesion c_s was determined by jointly considering the displacements at critical points and yield states of the sill mat. The numerical results show that the sill mats can apparently have different modes of failure, but the actual failure mechanism controlling the stability of sill mats is the crushing or shearing due to the closure of rock walls associated with the excavation of the underneath excavation. When this failure mechanism along with the Mitchell's failure mechanisms are considered, the increase of a stress in the sill mat does not always mean an improvement or deterioration of the stability of the sill mat. An increase of the horizontal stress tends to decrease the stability if the failure mechanism is horizontal crushing, but increases the stability if the flexural failure governs. Similarly, the vertical stresses (exercised by the overlying uncemented backfill) tend to destabilize the sill mats if the flexure controls the stability, while it plays a role of confining stress and thus stabilizes the sill mats in the case of horizontal crushing.

As the stability of the sill mat upon base-exposure is governed by the mechanism of crushing or shearing associated with the wall closure, it is straightforward to see an increase in the critical (or minimum required) cohesion as the mine depth z or rock stress ratio K_r increases. Results also showed that the critical cohesion increases as the stope width W or inclination angle β decreases. With higher uncemented backfill above the sill mat, one should expect larger critical cohesion c_s for the sill mat. With a thicker sill mat, the critical cohesion decreases. This trend corresponds well to that shown in the abacus of Pakalnis et al.[30], which does not consider the effect of mine depth. An increase in the Young's modulus of the sill mat E_s leads to an increase in the critical cohesion c_s, while an increase in the Young's modulus of the rock mass E_r leads to a decrease of the critical cohesion c_s.

Conflict of interest

The authors wish to confirm that there are no known conflicts of interest associated with this publication and there has been no significant financial support for this work that could have influenced its outcome.

Acknowledgements

The authors acknowledge the financial support from the Natural Sciences and Engineering Research Council of Canada (NSERC 402318), Fonds de recherche du Québec - Nature et Technologies (FRQNT 2015-MI-191676), Mitacs Elevate Post-doctoral Fellowship (IT08484), and the partners of the Research Institute on Mines and Environment (RIME UQAT-Polytechnique; http://rime-irme.ca/).

References

1. Hassani F, Archibald J. Mine backfill. Canadian Institute of Mining, Metallurgy and Petroleum, Montreal; 1998 [CD-ROM].
2. Aubertin M, Bernier L, Bussière B. Environnement et gestion des rejets miniers. Mont-Royal, Canada: Presses Internationales Polytechnique; 2002 [CD-ROM].
3. Darling, P. (Ed.). SME mining engineering handbook (Vol. 1). SME; 2011.
4. Hustrulid WA, Bullock RL. (eds.) (2001) Underground Mining Methods: Engineering Fundamentals and International Case Studies. SME: Littleton.
5. Donovan J, Dawson J, Bawden WF. David Bell Mine underhand cut and fill sill mat test. In Proceedings of the 9th International Symposium in Mining with Backfill, Montreal, Canada (Vol. 29); 2007.
6. Tesarik DR, Seymour JB, Yanske TR. Long-term stability of a backfilled room-and-pillar test section at the Buick Mine, Missouri, USA. Int J Rock Mech Min Sci 2009; 46(7): 1182-1196.
7. Mitchell RJ. Sill mat evaluation using centrifuge models. Min Sci Technol 1991; 13(3): 301-313.
8. Oulbacha Z. Analyse numérique de la stabilité des piliers-dalles en remblai cimenté : une vérification des modèles de Mitchell. MS Thesis, Montréal, Canada: École Polytechnique Montréal; 2014.
9. Caceres C. Effect of delayed backfill on open stope mining methods. Doctoral dissertation, Vancouver, Canada: University of British Columbia; 2005.
10. Caceres C, Moffat R, Pakalnis R. Evaluation of flexural failure of sill mats using classical beam theory and numerical models. Int J Rock Mech Min Sci 2017; 99: 21-27.
11. Mitchell, R. J., Olsen, R. S., and Smith, J. D. Model studies on cemented tailings used in mine backfill. Can. Geotech. J. 1982; 19(1):14-28.
12. Sobhi MA, Li, L. Numerical investigation of the stresses in backfilled stopes overlying a sill mat. J Rock Mech Geotech Eng 2017; 9(3): 490-501.
13. Dirige PA, De Souza E. Engineering design of backfill systems in undercut mining. Proceedings of the 9th International Symposium in Mining with Backfill (Minefill 2007). Montreal, Canada; 2007.
14. Brummer RK, Andrieux PP, O'Connor CP. Stability analyses of undermined sill mats for base metal mining. In: Brummer et al. (eds), FLAC and Numerical Modelling in Geomechanics. Swets and Zeitlinger: Lisse; 2003. p. 189-195.
15. Hughes P. Design guidelines: underhand cut and fill cemented paste backfill sill beams. Doctoral dissertation, Vancouver, Canada: University of British Columbia; 2014.
16. Brinkgreve RBJ, Vermeer PA. (Eds.). Plaxis: Finite Element Code for Soil and Rock Analyses: Version 7: [user's Guide]. Balkema; 1999.
17. Sobhi, Mohamed Amine. Analyse numérique visant l'évaluation du coefficient de pression des terres et des contraintes dans des chantiers remblayés au-dessus d'un pilier-dalle. Master thesis, École Polytechnique de Montréal, 2014.

18. Pagé P. Évaluation numérique de la stabilité des chantiers: Contraintes élastiques autour des chantiers et résistance nécessaire des semelles en remblai cimenté. MS Thesis, Montréal, Canada: École Polytechnique Montréal; 2018.
19. Fahey M, Helinski M, Fourie A. Some aspects of the mechanics of arching in backfilled stopes. Can Geotech J 2009 : 46 (11), 1322-1336.
20. Mitchell RJ, Wong BC. Behaviour of cemented tailings sands. Can Geotech J 1982: 19(3): 289-295.
21. Koupouli NJ, Belem T, Rivard P, Effenguet H. Direct shear tests on cemented paste backfill–rock wall and cemented paste backfill–backfill interfaces. J Rock Mech Geotech Eng 2016; 8(4): 472-479.
22. Herget G. Stresses in rock. Rotterdam: Balkema; 1988.
23. Liu, G, Li L, Yang X, Guo L. Stability analyses of vertically exposed cemented backfill: A revisit to Mitchell's physical model tests. Int J Min Sc. Technol 2016; 26(6): 1135-1144.
24. Sobhi MA, Li L, Aubertin M. Numerical investigation of the earth pressure coefficient along the central line of backfilled stopes. Can Geotech J 2017; 54: 138-145.
25. Yan ZX, Duan J, Wang HY. Constitutive models in stability analysis of rock slope. J Central South Uni Technol 2008; 15(1): 302-306.
26. Su K, Li Y. Discussion of extended Drucker-Prager yield criterion in slope stability analysis. In: Power and Energy Engineering Conference, 2009. APPEEC 2009. Asia-Pacific (pp. 1-4). IEEE.
27. Yang P, Li L, Aubertin M, Brochu-Baekelmans M, Ouellet S. Stability analyses of waste rock barricades designed to retain paste backfill. Int J Geomech 2017; 17(3): 04016079.
28. Yang P, Li L, Aubertin M. A new solution to assess the required strength of mine backfill with a vertical exposure. Int J Geomech 2017; 17(10), 04017084.
29. Liu, G, Li L, Yang X, Guo L. Required strength estimation of a cemented backfill with the front wall exposed and back wall pressured. Int. J. Min and Mineral Eng 2018 (in press).
30. Pakalnis R, Caceres C, Clapp K, Morin M, Brady T, Williams T. MacLaughlin M. Design spans-underhand cut and fill mining. In: Proceedings of 107th CIM-AGM. Toronto; 2005.
31. Stone DMR. The optimization of mix designs for cemented rockfill. In: Minefill; 1993. p. 249-253.
32. Salencon, J. Contraction quasi-statique d'une cavité a symétrie sphérique ou cylindrique dans un milieu elastoplastique. Annales Des Ponts Et Chaussées 1969; 4:231-236.
33. Hoek E, Carranza-Torres C, Corkum, B. (2002). Hoek-Brown failure criterion-2002 edition. In: Proceedings of NARMS-Tac; 2002. (1) 267-273.
34. Liu, G., Li, L., Yang, X., and Guo, L. A numerical analysis of the stress distribution in backfilled stopes considering nonplanar interfaces between the backfill and rock walls. Int. J. Geotech. Eng. 2016; 10(3): 271-282.
35. Liu, G., Li, L., Yang, X., and Guo, L. Numerical analysis of stress distribution in backfilled stopes considering interfaces between the backfill and rock walls. Int. J. Geomech. 2017; 10.1061/(ASCE)GM.1943-5622.0000702, 06016014.
36. Li, L, Aubertin M. Numerical investigation of the stress state in inclined backfilled stopes. Int J Geomech 2009; 9(2): 52-62.
37. Falaknaz N, Aubertin M, Li L. Numerical investigation of the geomechanical response of adjacent backfilled stopes. Can. Geotech. J 2015; 52(10): 1507-1525.
38. Sainsbury DP, Urie R. Stability analysis of horizontal and vertical paste fill exposures at the Raleigh Mine. Proc., 9th Int. Symp. on Mining with Backfill, Montreal; 2007.
39. Li, L, Aubertin M, Shirazi A. Implementation and application of a new elastoplastic model based on a multiaxial criterion to assess the stress state near underground openings. Int J Geomech 2010; 10(1): 13-21.